Efficiency enhancement of organic light-emitting devices due to a localized surface plasmonic resonance effect of poly(4-butylphenyl-diphenyl-amine):dodecanethiol functionalized Au nanocomposites

Dae Hun Kim and Tae Whan Kim

Department of Electronics and Computer Engineering, Hanyang University, Seoul 133-791, South Korea
**twk@hanyang.ac.kr*

Abstract: Organic light-emitting devices (OLEDs) were fabricated utilizing a poly(4-butylphenyl-diphenyl-amine) (poly-TPD):dodecanethiol functionalized Au (DDT-Au) nanocomposite (NC) layer to enhance their current efficiency. The photoluminescence intensity of the poly-TPD:DDT-Au NC film at 514 nm was significantly increased, being about 1.3 times that of the poly-TPD film due to the coupling between the excitons in the emitting layer and the localized surface plasmonic resonance of the DDT-Au nanoparticles. The current efficiency of the green OLEDs with a poly-TPD:DDT-Au NC layer at 1000 cd/m^2 was 3.1 cd/A larger than that with a poly-TPD layer, resulting in an enhanced out-coupling efficiency due to the coupling effect.

OCIS codes: (230.0230) Optical devices; (240.6680) Surface plasmons; (230.3670) Light-emitting diodes.

References and links

1. S. Höfle, M. Pfaff, H. Do, C. Bernhard, D. Gerthsen, U. Lemmer, and A. Colsmann, "Suppressing molecular aggregation in solution processed small molecule organic light emitting diodes," Org. Electron. **15**(1), 337–341 (2014).
2. S. Höfle, M. Bruns, S. Strässle, C. Feldmann, U. Lemmer, and A. Colsmann, "Tungsten oxide buffer layers fabricated in an inert sol-gel process at room-temperature for blue organic light-emitting diodes," Adv. Mater. **25**(30), 4113–4116 (2013).
3. T. Chiba, Y. J. Pu, R. Miyazaki, K. Nakayama, H. Sasabe, and J. Kido, "Ultra-high efficiency by multiple emission from stacked organic light-emitting devices," Org. Electron. **12**(4), 710–715 (2011).
4. A. Kumar, R. Srivastava, P. Tyagi, D. S. Mehta, and M. N. Kamalasanan, "Effect of doping of 8-hydroxyquinolinatolithium on electron transport in tris(8-hydroxyquinolinato)aluminum," J. Appl. Phys. **109**(11), 114511 (2011).
5. D. H. Kim and T. W. Kim, "Efficiency enhancement in tandem organic light-emitting devices with a hybrid charge generation layer composed of BEDT-TTF-doped TPBi/mCP/HAT-CN," Org. Electron. **15**(12), 3452–3457 (2014).
6. Y. H. Lee, D. H. Kim, K.-H. Yoo, and T. W. Kim, "Efficiency enhancement of organic light-emitting devices due to the localized surface plasmonic resonant effect of Au nanoparticles embedded in ZnO nanoparticles," Appl. Phys. Lett. **105**(18), 183303 (2014).
7. S. R. Forrest, D. D. C. Bradley, and M. E. Thompson, "Measuring the efficiency of organic light-emitting devices," Adv. Mater. **15**(13), 1043–1048 (2003).
8. F. B. Dias, K. N. Bourdakos, V. Jankus, K. C. Moss, K. T. Kamtekar, V. Bhalla, J. Santos, M. R. Bryce, and A. P. Monkman, "Triplet harvesting with 100% efficiency by way of thermally activated delayed fluorescence in charge transfer OLED emitters," Adv. Mater. **25**(27), 3707–3714 (2013).
9. E. L. Williams, K. Haavisto, J. Li, and G. E. Jabbour, "Excimer-based white phosphorescent organic light-emitting diodes with nearly 100% internal quantum efficiency," Adv. Mater. **19**(2), 197–202 (2007).
10. S. O. Jeon, K. S. Yook, C. W. Joo, and J. Y. Lee, "Theoretical maximum quantum efficiency in red phosphorescent organic light-emitting diodes at a low doping concentration using a spirobenzofluorene type triplet host material," Org. Electron. **11**(5), 881–886 (2010).

#234901 - $15.00 USD Received 17 Feb 2015; revised 10 Apr 2015; accepted 12 Apr 2015; published 21 Apr 2015

11. F. Kessler, Y. Watanabe, H. Sasabe, H. Katagiri, M. K. Nazeeruddin, M. Grätzel, and J. Kido, "High-performance pure blue phosphorescent OLED using a novel bis-heteroleptic iridium(III) complex with fluorinated bipyridyl ligands," J. Mater. Chem. C **1**(6), 1070–1075 (2013).
12. S. Y. Kim, W. I. Jeong, C. Mayr, Y. S. Park, K. H. Kim, J. H. Lee, C. K. Moon, W. Brütting, and J. J. Kim, "Organic light-emitting diodes with 30% external quantum efficiency based on a horizontally oriented emitter," Adv. Funct. Mater. **23**(31), 3896–3900 (2013).
13. H.-W. Chang, J. Lee, S. Hofmann, Y. Hyun Kim, L. Müller-Meskamp, B. Lüssem, C.-C. Wu, K. Leo, and M. C. Gather, "Nano-particle based scattering layers for optical efficiency enhancement of organic light-emitting diodes and organic solar cells," J. Appl. Phys. **113**(20), 204502 (2013).
14. T. Bocksrocker, J. Hoffmann, C. Eschenbaum, A. Pargner, J. Preinfalk, F. Maier-Flaig, and U. Lemmer, "Micro-spherically textured organic light emitting diodes: a simple way towards highly increased light extraction," Org. Electron. **14**(1), 396–401 (2013).
15. H.-W. Chang, Y. H. Kim, J. Lee, S. Hofmann, B. Lüssem, L. Müller-Meskamp, M. C. Gather, K. Leo, and C.-C. Wu, "Color-stable ITO-free white organic light-emitting diodes with enhanced efficiency using solution-processed transparent electrodes and optical outcoupling layers," Org. Electron. **15**(5), 1028–1034 (2014).
16. F. Li, X. Li, J. Zhang, and B. Yang, "Enhanced light extraction from organic light-emitting devices by using microcontact printed silica colloidal crystals," Org. Electron. **8**(5), 635–639 (2007).
17. K. U. Yang, K. C. Choi, and C. W. Ahn, "Surface plasmon-enhanced spontaneous emission rate in an organic light-emitting device structure: Cathode structure for plasmonic application," Appl. Phys. Lett. **94**(17), 173301 (2009).
18. A. Fujiki, T. Uemura, N. Zettsu, M. Akai-Kasaya, A. Saito, and Y. Kuwahara, "Enhanced fluorescence by surface plasmon coupling of Au nanoparticles in an organic electroluminescence diode," Appl. Phys. Lett. **96**(4), 043307 (2010).
19. Y. Xiao, J. P. Yang, P. P. Cheng, J. J. Zhu, Z. Q. Xu, Y. H. Deng, S. T. Lee, Y. Q. Li, and J. X. Tang, "Surface plasmon-enhanced electroluminescence in organic light-emitting diodes incorporating Au nanoparticles," Appl. Phys. Lett. **100**(1), 013308 (2012).
20. F. Yan and X. W. Sun, "A plasmonically enhanced charge generation layer for tandem organic light emitting device," Appl. Phys. Lett. **102**(4), 043303 (2013).
21. F. Liu and J.-M. Nunzi, "Phosphorescent organic light emitting diode efficiency enhancement using functionalized silver nanoparticles," Appl. Phys. Lett. **99**(12), 123302 (2011).
22. K. Xu, Y. Li, W. Zhang, L. Zhang, and W. Xie, "Effect of gold nanoparticles on the performances of the phosphorescent organic light-emitting devices," Curr. Appl. Phys. **14**(1), 53–56 (2014).
23. T. Tanaka, Y. Totoki, A. Fujiki, N. Zettsu, Y. Miyake, M. Akai-Kasaya, A. Saito, T. Ogawa, and Y. Kuwahara, "Enhanced red-light emission by local plasmon coupling of Au nanorods in an organic light-emitting diode," Appl. Phys. Express **4**(3), 032105 (2011).
24. M. Jung, D. M. Yoon, M. Kim, C. Kim, T. Lee, J. H. Kim, S. Lee, S.-H. Lim, and D. Woo, "Enhancement of hole injection and electroluminescence by ordered Ag nanodot array on indium tin oxide anode in organic light emitting diode," Appl. Phys. Lett. **105**(1), 013306 (2014).
25. A. Kumar, R. Srivastava, P. Tyagi, D. S. Mehta, and M. N. Kamalasanan, "Efficiency enhancement of organic light emitting diode via surface energy transfer between exciton and surface plasmon," Org. Electron. **13**(1), 159–165 (2012).
26. J. W. Zhang, Y. He, X. Q. Chen, Y. Pei, H. M. Yu, J. J. Qin, and X. Y. Hou, "Study on the basic capacitance–voltage characteristics of organic molecular semiconductors," Org. Electron. **21**, 73–77 (2015).
27. S.-F. Chen and C.-W. Wang, "Influence of the hole injection layer on the luminescent performance of organic light emitting diodes," Appl. Phys. Lett. **85**(5), 765–767 (2004).

1. Introduction

Organic light-emitting devices (OLEDs) have been receiving considerable attention for potential applications in flexible displays and solid-state lighting [1–4]. The prospect of promising applications of OLEDs has led to substantial research and development efforts to enhance their efficiency [5,6] The external quantum efficiency of the OLEDs is significantly affected by various factors of the internal quantum efficiency, such as the charge balance factor, the spin static factor, the photoluminescence efficiency, and the out-coupling efficiency [7]. While the internal quantum efficiency of OLEDs fabricated utilizing phosphorescent materials is approximately 100% [8–11], the external quantum efficiency of OLEDs is still relatively low due to the poor out-coupling efficiency of approximately 30% [12–15]. Various techniques have been suggested to increase the out-coupling efficiency in OLEDs [16]. Many studies concerning OLEDs utilizing metal nanoparticles (NPs) have been performed to increase the out-coupling efficiency [17–24]. The effect of the electromagnetic field on the metal NPs produces an intense absorption, resulting in the formation of a localized surface plasmonic resonance (LSPR), which acts as a collective oscillation of the electrons on the surfaces of the NPs. The efficiency enhancement of OLEDs utilizing metal NPs originates from the effective coupling between the emission of the emitting layer (EML)

#234901 - $15.00 USD Received 17 Feb 2015; revised 10 Apr 2015; accepted 12 Apr 2015; published 21 Apr 2015

and the LSPR of the Au NPs [25]. Some works on enhancing the light emission in OLEDs fabricated utilizing Au NPs have been conducted. An increase of 25% in the electroluminescence (EL) intensity and efficiency by incorporating synthesized Au NPs into poly(3,4-ethylenedioxythiophene)-poly(styrenesulfonate) has been reported [18]. Even though some studies on the enhanced efficiency of the EL intensity for OLEDs utilizing Au NPs based on tris(8-hydroxylquinolianato)aluminum (III) have been suggested [19], the morphology of the hole-injection layer (HIL) with embedded Au NPs is poor due to an agglomeration of the Au NPs, thus limiting the performance limitation of the OLEDs. Therefore, investigations of the enhanced efficiency of OLEDs made with nanocomposites are necessary to enhance device efficiency.

This paper reports data on the performance enhancement of OLEDs fabricated utilizing a poly(4-butylphenyl-diphenyl-amine) (poly-TPD):dodecanethiol functionalized Au (DDT-Au) nanocomposite (NC) layer. Transmission electron microscopy (TEM) and atomic force microscopy (AFM) measurements were performed to investigate the structural properties and the surface morphologies of the poly-TPD and the poly-TPD:DDT-Au NC films. Ultraviolet photoelectron spectroscopy (UPS) measurements were performed to investigate the variations in the energy bands for the poly-TPD and the poly-TPD:DDT-Au NC films. Absorption, photoluminescence (PL), and time-resolved photoluminescence (TRPL) measurements were carried out to investigate the mechanisms for the coupling between the exciton in the EML and the LSPR of the poly-TPD:DDT-Au NC layer. Current density - voltage - luminance measurements were carried out to investigate the electrical and the optical properties of the OLEDs fabricated utilizing a poly-TPD:DDT-Au NC layer. The effects of the DDT-Au NPs embedded in the poly-TPD layer on the current efficiency of OLEDs were investigated to clarify their impact on the performances of the devices.

2. Experimental Details

The sheet resistivity and the thickness of the indium-tin-oxide (ITO) thin films coated on glass substrates were 15 ohm/square and 150 nm, respectively. The ITO-coated glass substrates were cleaned in acetone and methanol at 25°C for 20 min by using an ultrasonic cleaner and were thoroughly rinsed in de-ionized water. After the chemically-cleaned ITO-coated glass substrates had been dried by using N_2 gas with a purity of 99.999%, the surfaces of the ITO-coated glass substrates were treated with an ultraviolet-ozone gas for 20 min at room temperature. After a blend of the poly-TPD (12 mg/mL) and the DDT-Au NPs (0.48 mg/mL) had been dissolved in chlorobenzene, the solution was stirred for 24 h at 60°C. The blend solution was deposited onto the ITO-coated glass substrates by using a spin-coating method at 5000 rpm for 60 s and was annealed at 145°C for 30 min in a glove box. After the samples with a poly-TPD:DDT-Au NC layer on an ITO-coated glass substrate had been transferred into an evaporation chamber, the organic layers and the electrodes were deposited at a substrate temperature of 25°C and a system pressure of 1.7×10^{-4} Pa. The deposition rates of the organic layers and the metal layer were approximately 1.0 and 2.0 Å/s, respectively. The TEM samples were prepared by the spin coating method. The blend solution was deposited onto the copper grid attached glass at 5000 rpm for 60 s and was annealed at 145°C for 30 min in a glove box. The AFM samples were spin-coated onto the ITO-glass at 5000 rpm for 60 s and were annealed at 145°C for 30 min in a glove box. The poly-TPD:DDT-Au NC film for the PL measurements was spin-coated onto the glass at 5000 rpm for 60 s, and the 4,4′-Bis(N-carbazolyl)-1,1′-biphenyl (CBP):tris[2-phenylpyridinato-C2,N]iridium ($Ir(ppy)_3$) was deposited into an evaporation chamber. The PL pulse laser was irradiated onto CBP: $Ir(ppy)_3$/poly-TPD:DDT-Au NC film. The PL spectroscopy measurements were performed by using a time-correlated single photon counting method. The TEM and the AFM images were measured by using a JEM 2100F transmission electron microscope operating at 200 kV and an XE-100 atomic force microscope, respectively. The UPS spectra were measured by using a theta probe base system purchased from the Thermo Fisher Scientific Co. The UPS spectra were obtained with a He I 21.2-eV source. The absorption spectra were measured by using a VARIAN Cary 100 Conc UV/vis

#234901 - $15.00 USD Received 17 Feb 2015; revised 10 Apr 2015; accepted 12 Apr 2015; published 21 Apr 2015

spectrophotometer. PL and TRPL spectroscopy measurements were performed by using an X-ray fluorescence spectrometer (TCSPC-FL920) equipped with a pulse laser operating at 370 nm.

The current-voltage characteristics were measured on a programmable electrometer with built-in current and voltage measurement units (M6100, McScience). The brightness was measured by using a brightness meter, and the EL spectra were measured by using a luminescence spectrometer (CS-1000, Minolta).

3. Results and Discussion

Figures 1(a) and 1(b) show the chemical structures of the poly-TPD and the DDT-Au NPs, respectively.

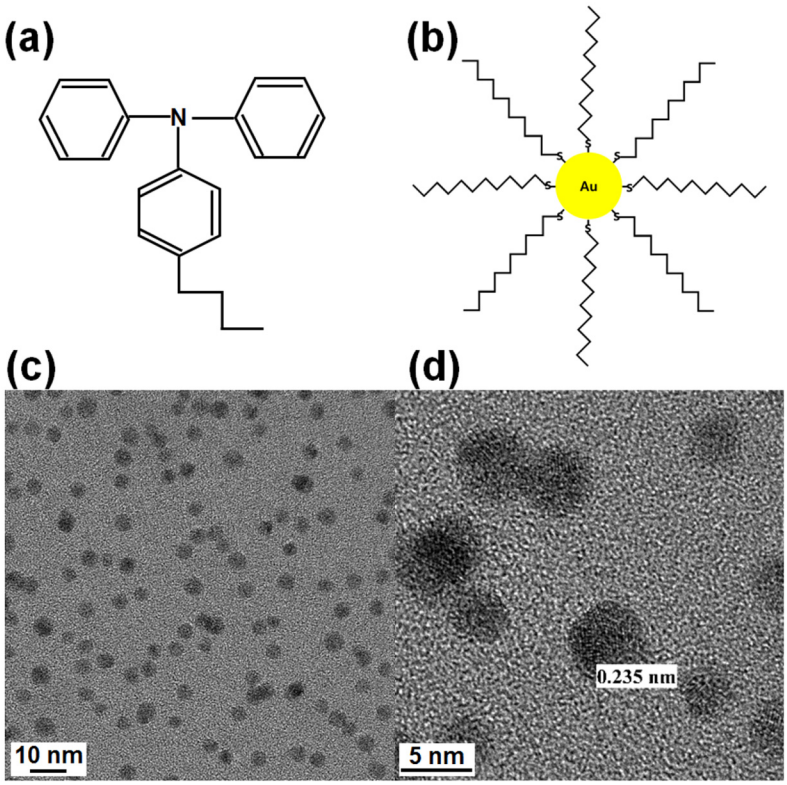

Fig. 1. Schematic diagrams of the chemical structures for the (a) poly-TPD and the (b) DDT-Au nanoparticles. (c) Low-magnification transmission electron microscopy image and (d) high-magnification transmission electron microscopy image of the poly-TPD:DDT-Au nanocomposite film.

Because the DDT ligands of the DDT-Au NPs are reversible from the hydrophilic Au NPs to the hydrophobic DDT-Au NPs, the DDT-Au NPs are uniformly dispersed in the poly-TPD. The DDT-Au NPs are attached to the surface of the poly-TPD film due to the interactions between the DDT ligands of the DDT-Au NPs and the chains of the poly-TPD. Figures 1(c) and 1(d) show TEM images of the poly-TPD film and the poly-TPD:DDT-Au nanocomposite film, respectively. The low-magnification TEM image of the Fig. 1(c) shows that the DDT-Au NPs are uniformly dispersed in the poly-TPD film due to the DDT ligands on the surfaces of the DDT-Au NPs. The agglomeration of the Au NPs is decreased due to the combination between the chains of the poly-TPD and the DDT ligands on the surfaces of the DDT-Au NPs. The high-magnification TEM image of the Fig. 1(d) shows that the average size of the DDT-Au NPs is approximately 5 nm. The lattice fringe of the Au NPs, as determined from

#234901 - $15.00 USD Received 17 Feb 2015; revised 10 Apr 2015; accepted 12 Apr 2015; published 21 Apr 2015

Fig. 1(d), is about 0.235 nm, and the planes with an interplanar distance of 0.235 nm correspond to the (111) planes of the cubic Au phase.

Figure 2 shows AFM images of (a) the poly-TPD film and (b) the poly-TPD:DDT-Au NC film, and (c)-(d) show the profile images corresponding to (a) and (b), respectively. The root-mean-square roughness values of the poly-TPD and the poly-TPD:DDT-Au NC films are 0.24 and 0.25 nm, respectively, as shown in Figs. 2(a) and 2(d). The peak-to-valley roughnesses of the poly-TPD and the poly-TPD:DDT-Au NC films are 1.17 and 1.52 nm, respectively, as shown in Figs. 2(c) and 2(d). The morphology of the poly-TPD:DDT-Au NC film is as smooth as that of the poly-TPD film due to the uniform dispersion of the DDT-Au NPs embedded in the poly-TPD.

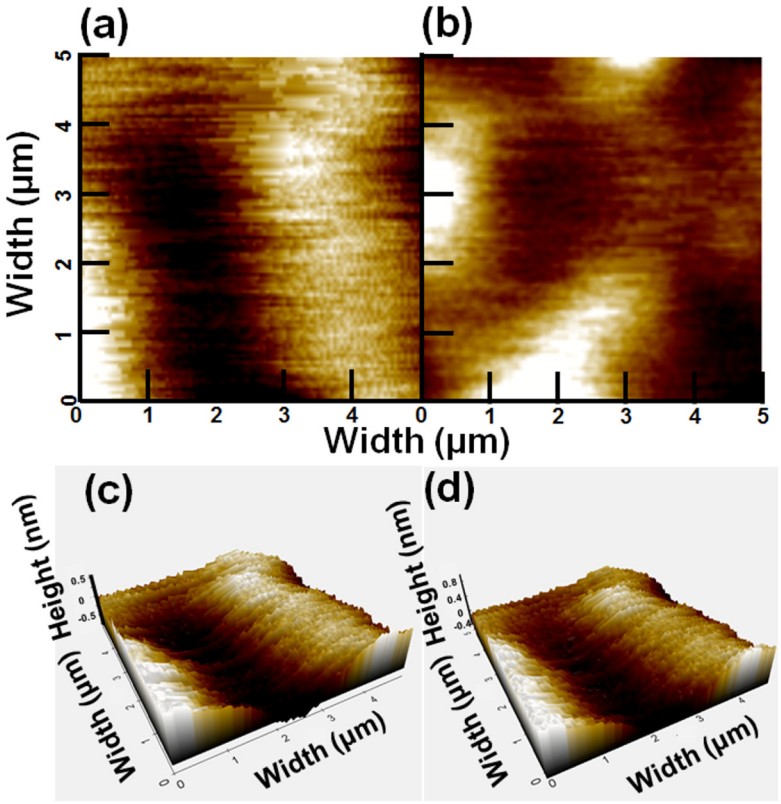

Fig. 2. Atomic force microscopy (AFM) images of the (a) poly-TPD film and the (b) poly-TPD:DDT-Au nanocomposite film. (c)-(d) Corresponding profile images of the AFM images in (a) and (b).

Figure 3 shows the UPS spectra of the poly-TPD and the poly-TPD:DDT-Au NC films. The highest occupied molecular orbital (HOMO) edges of the poly-TPD and the poly-TPD:DDT-Au NC films are located at 5.1 and 5.2 eV below the Fermi energy, respectively. This result indicates that the DDT-Au NPs embedded in the poly-TPD layer do not affect the energy level of the poly-TPD.

#234901 - $15.00 USD Received 17 Feb 2015; revised 10 Apr 2015; accepted 12 Apr 2015; published 21 Apr 2015

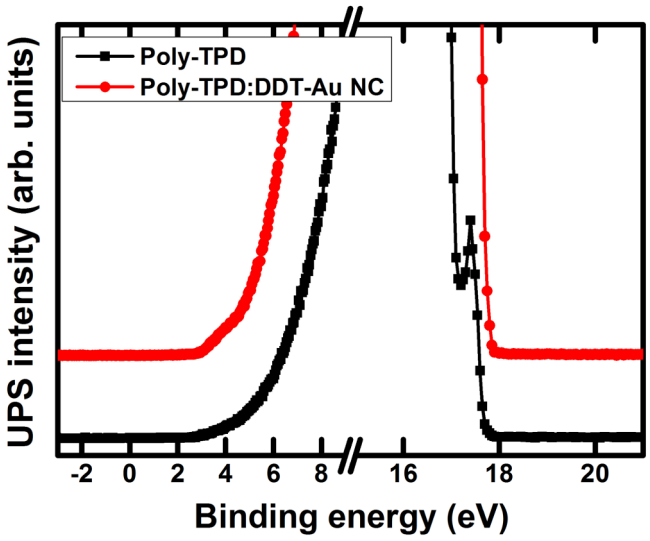

Fig. 3. Ultraviolet photoelectron spectroscopy spectra of the poly-TPD film and the poly-TPD:DDT-Au nanocomposite film.

Figure 4 shows the current density - voltage characteristics of hole-only devices without a HIL, with a poly-TPD layer and with a poly-TPD:DDT-Au NC layer.

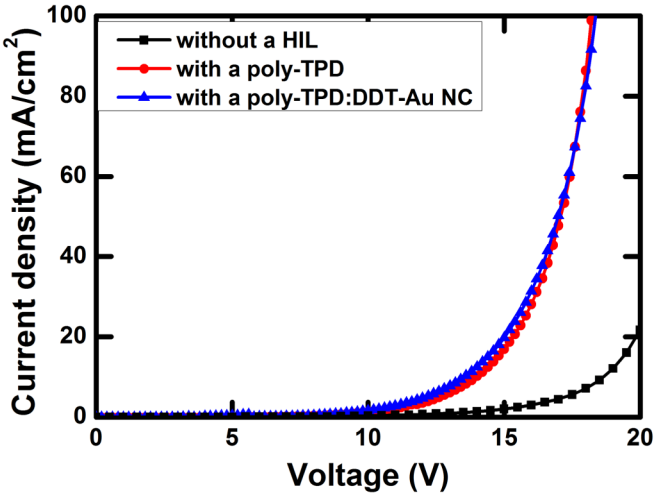

Fig. 4. Current density - voltage characteristics of the hole-only devices without a hole-injection layer, with a poly-TPD layer, and a poly-TPD:DDT-Au nanocomposite.

The structures of the hole-only devices consist of an ITO-coated glass substrate/no HIL, a poly-TPD layer and a poly-TPD:DDT-Au NC layer (40 nm)/an N,N′-di(1-naphthyl)-N,N′-diphenyl-(1,1′-biphenyl)-4,4′-diamine (NPB) layer (100 nm)/an Al electrode. Hole-only devices without a HIL, with a poly-TPD layer and with poly-TPD:DDT-Au NC layer were fabricated to investigate the number of holes injected from the ITO electrode into the EML. The operating voltages of the hole-only devices without a HIL, with a poly-TPD layer and with a poly-TPD:DDT-Au NC layer at 10 mA/cm^2 were 18.6, 13.9, and 13.5 V, respectively. The operating voltage of the hole-only device with a poly-TPD layer was 4.7 V smaller than that of the hole-only device without a HIL. The HOMO levels of the NPB and the poly-TPD are 5.5 and 5.1 eV, respectively [26]. The HOMO level of the poly-TPD is located between

#234901 - $15.00 USD Received 17 Feb 2015; revised 10 Apr 2015; accepted 12 Apr 2015; published 21 Apr 2015

the work function of the ITO and the HOMO level of the NPB, resulting in the enhancement of the hole injection efficiency. Furthermore, the smooth surface of the poly-TPD/ITO films might provide a uniform conducting path for holes to cross the ITO/HIL interface, leading to decreasing an operating voltage [27]. The operating voltage of the hole-only device with a poly-TPD:DDT-Au NC layer was almost the same as that of the hole-only device with a poly-TPD layer.

Figure 5 shows the (a) schematic diagram of the structure of the poly-TPD:DDT-Au NC film, the (b) absorption spectra of the poly-TPD and the poly-TPD:DDT-Au NC films, the (c) PL spectra of the CBP:Ir(ppy)$_3$ EML on the poly-TPD film and on the poly-TPD:DDT-Au NC film, and the (d) TRPL spectra of CPB:Ir(ppy)$_3$ EML on the poly-TPD film and on the poly-TPD:DDT-Au NC film.

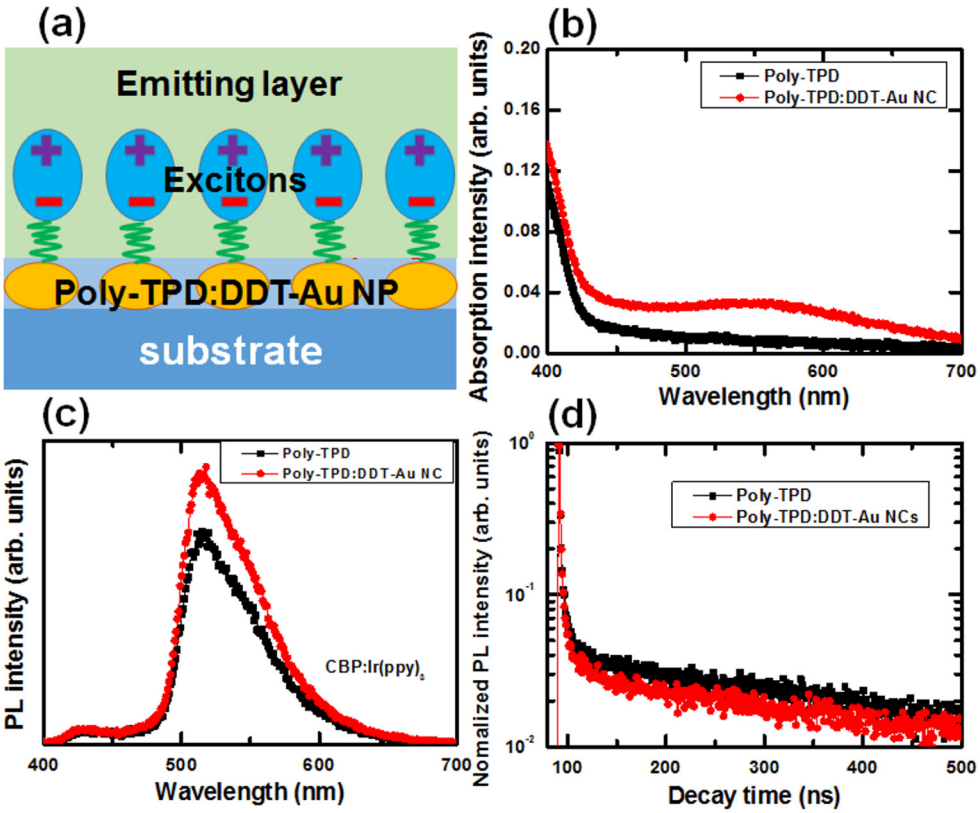

Fig. 5. (a) Schematic diagram of the poly-TPD:DDT-Au nanocomposite film, (b) absorption spectra of the poly-TPD film and the poly-TPD:DDT-Au nanocomposite film, and (c) photoluminescence and (d) time-resolved photoluminescence spectra of the CBP:Ir(ppy)$_3$ emitting layer on the poly-TPD layer and on the poly-TPD:DDT-Au nanocomposite layer.

The sample structures of the CBP:Ir(ppy)$_3$ EML on the poly-TPD film and on the poly-TPD:DDT-Au NC film ITO-coated glass substrates describe the coupling mechanisms between the excitons of the EML and the LSPR of the DDT-Au NPs, as shown in Fig. 5(a). When the local electromagnetic field of the excitons in the EML overlaps that of the LSPR of the DDT-Au NPs in the poly-TPD film, a coupling between the excitons and the LSPR occurs due to the effective energy transfer that takes place between the excitons and the LSPR, resulting in the creation of the alternate channel for emission. Because the scattering speed of the LSPR with a high momentum is much faster than the decay of the excitons, the coupling between the excitons and the LSPR enhances the radiation's intensity [25]. Figure 5(b) shows the absorption spectra of the poly-TPD and the poly-TPD:DDT-Au NC films. The peak of the

#234901 - $15.00 USD Received 17 Feb 2015; revised 10 Apr 2015; accepted 12 Apr 2015; published 21 Apr 2015

absorption intensity of the poly-TPD:DDT-Au NC film, which occurs at a wavelength between 500 and 600 nm, is larger than that of the poly-TPD film due to the enhanced absorption of the DDT-Au NPs. The dominant absorption region corresponds to the LSPR wavelength of the DDT-Au NPs. Coupling behaviors between the excitons in the EML and the LSPR of the DDT-Au NPs significantly affect the spontaneous emission rate. When the wavelength of the absorption spectrum of the LSPR at the DDT-Au NPs matches that of the emission spectrum, the dominant PL peak at 514 nm corresponds to the emitting frequency of the CBP:Ir(ppy)$_3$ EML and results an enhanced efficiency, as shown in Fig. 5(c). The PL peak at 514 nm for the CBP:Ir(ppy)$_3$ EML is close to the increased absorption region for the poly-TPD:DDT-Au NCs corresponding to the LSPR of the DDT-Au-NPs, thereby causing a coupling between the excitons and the LSPR. The PL decay time of the poly-TPD:DDT-Au NC film is much faster than that of the poly-TPD film due to the coupling process, as shown in Fig. 5(d), resulting in an enhanced radiative intensity. The PL intensity of the poly-TPD:DDT-Au NC film at 514 nm is 1.3 times that of the poly-TPD film, as shown in Fig. 5(c). The increase in the PL intensity for the poly-TPD:DDT-Au NC film is attributed to an effective energy transfer between the radiated light generated in the CBP:Ir(ppy)$_3$ EML and the LSPR excited by the DDT-Au NPs in the poly-TPD film.

Figure 6 shows the (a) current density - voltage, the (b) luminance - voltage, the (c) current efficiency - luminance, and the (d) normalized EL spectra of the green and blue OLEDs with a poly-TPD layer and a poly-TPD:DDT-Au NC layer.

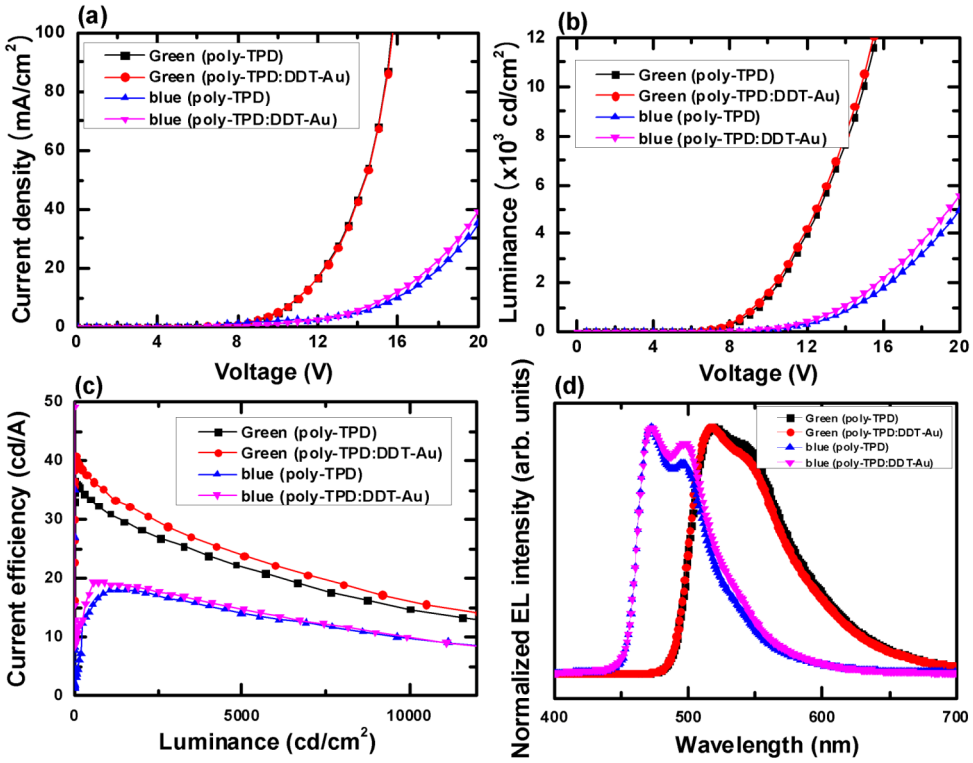

Fig. 6. (a) Current density - voltage, (b) luminance - voltage, (c) current efficiency - luminance characteristics, and (d) normalized electroluminescence spectra of the green and blue OLEDs with a poly-TPD layer and a poly-TPD:DDT-Au nanocomposite layer.

The OLEDs consist of ITO-coated glass substrate/poly-TPD layer or poly-TPD:DDT-Au NC layer (40 nm)/4,4'-cyclohexylidenebis[N,N-bis(4-methylphenyl)benzenamine (TAPC) hole transport layer (HTL) (20 nm)/CBP:Ir(ppy)$_3$ or 1,3-Bis(N-carbazolyl)benzene:bis[2-(4,6-difluorophenyl)pyridinato-C2,N](picolinato)iridium(III) EML (30 nm)/1,3,5-tris(1-phenyl-1h-

#234901 - $15.00 USD Received 17 Feb 2015; revised 10 Apr 2015; accepted 12 Apr 2015; published 21 Apr 2015

benzimidazol-2-yl)benzene electron transport layer (30 nm)/LiF electron injection layer (1 nm)/Al electrode (100 nm). The efficiency of radiation enhancement may decrease sensitively as the distance between the EML and the poly-TPD:DDT-Au NC layer increases. The thickness of TAPC layer was chosen to be thin enough to have a meaningful LSPR coupling yet thick enough to maintain the chance of nonradiative exciton quenching low near metallic particles [25]. The operating voltages of the green OLEDs with a poly-TPD layer and a poly-TPD:DDT-Au NC layer at 10 mA/cm^2 are 9.6 and 9.6 V, respectively, and those of the blue OLEDs with a poly-TPD layer and a poly-TPD:DDT-Au NC layer at 10 mA/cm^2 are 15.8 and 15.5 V, respectively, as shown in Fig. 6(a). The operating voltages of the green and blue OLEDs with a poly-TPD layer and those with a poly-TPD:DDT-Au NC layer have almost the same value, indicating that the DDT-Au NPs do not affect the number of holes injected from the ITO electrode to the EML. The operating voltages of the green OLEDs with a poly-TPD layer and a poly-TPD:DDT-Au NC layer at 100 cd/cm^2 are 9.5 and 9.1 V, respectively, and those of the blue OLEDs with a poly-TPD layer and a poly-TPD:DDT-Au NC layer at 100 cd/cm^2 are 14.4 and 13.7 V, respectively, as shown in Fig. 6(b). The operating voltage of the green OLEDs with a poly-TPD:DDT-Au NC layer at 1000 cd/cm^2 is 0.4 V smaller than that of the OLEDs with a poly-TPD layer due to the coupling between the excitons of the EML and the LSPR of the poly-TPD:DDT-Au NCs. The operating voltage of the blue OLEDs with a poly-TPD:DDT-Au NC layer at 1000 cd/cm^2 is 0.7 V smaller than that of the OLEDs with a poly-TPD layer. The current efficiencies of the green OLEDs with a poly-TPD layer and a poly-TPD:DDT-Au NC layer at 1000 cd/m^2 are 31.2 and 34.3 cd/A, respectively, and those of the blue OLEDs with a poly-TPD layer and a poly-TPD:DDT-Au NC layer at 1000 cd/m^2 are 17.8 and 19.1 cd/A, respectively. The current efficiency of the green OLEDs with a poly-TPD:DDT-Au NC layer at 1000 cd/m^2 is 3.1 cd/A larger than that of the green OLEDs with a poly-TPD layer, as shown in Fig. 6(c), due to the enhanced luminance resulting from the occurrence of the energy transfer via the coupling between the excitons in the EML and the LSPR of the poly-TPD:DDT-Au NC layer. Figure 6(d) shows the normalized EL spectra for the green and blue OLEDs with a poly-TPD layer and a poly-TPD:DDT-Au NC layer. While the intensity of the dominant emission peak at 514 nm for the green OLEDs with a poly-TPD:DDT-Au NC layer is larger than that of the green OLEDs with a poly-TPD layer, the intensities of the shoulder emission peak at 500 and 528 nm for the blue OLEDs with a poly-TPD:DDT-Au NC layer is larger than those for the blue OLEDs with a poly-TPD layer due to the coupling effect of the DDT-Au NPs embedded in the poly-TPD layer.

4. Summary and Conclusions

The electrical and the optical properties of the green and blue OLEDs fabricated with a poly-TPD layer and a poly-TPD:DDT-Au NC layer were determined to clarify the origin of the efficiency enhancements. TEM and AFM images showed that the DDT-Au NPs were uniformly dispersed in the poly-TPD film due to the DDT ligands on the surfaces of the Au NPs, resulting in a smooth of morphology. The current characteristics of hole-only devices showed that the relative hole flow rate of the poly-TPD:DDT-Au NC film was similar to that of the poly-TPD film. The overlap between the absorption spectrum of the DDT-Au NPs in the poly-TPD film and the PL spectrum of the EML contributed to the coupling between the emission in the EML and the LSPR excited by the DDT-Au NPs in the poly-TPD film, resulting in an enhanced out-coupling efficiency. While the current efficiency of the green OLEDs with a poly-TPD:DDT-Au NC layer at 1000 cd/m^2 was 3.1 cd/A larger than that of the green OLEDs with a poly-TPD layer, the current efficiency of the blue OLEDs with a poly-TPD:DDT-Au NC layer at 1000 cd/m^2 was 1.3 cd/A larger than that of the green OLEDs with a poly-TPD layer. An increase in the EL intensity for the OLEDs with a poly-TPD:DDT-Au NC layer was strongly related to an effective energy transfer between the radiated light generated in the EML and the LSPR excited by the DDT-Au NPs in the poly-TPD layer.

#234901 - $15.00 USD Received 17 Feb 2015; revised 10 Apr 2015; accepted 12 Apr 2015; published 21 Apr 2015

Acknowledgments

This research was supported by Basic Science Research Program through the National Research Foundation of Korea (NRF) funded by the Ministry of Education, Science and Technology (2013-016467).

#234901 - $15.00 USD Received 17 Feb 2015; revised 10 Apr 2015; accepted 12 Apr 2015; published 21 Apr 2015